Self-Diffraction Characterization and Optical Limiting Behavior of the PAni/PVA Nanofiber

Rajaa M. Abdullah[a], **Mohammed T. Obeed**[a], **Zainab J. Sweah**[b], **Hussain A. Badran**[c,*],
Riyadh Ch. Abul-Hail[c], **and Maytham Qabel Hamzah**[d]

[a]*Department of Material Science, Polymer Research Center, University of Basrah, Basrah, Iraq*
[b]*Department of Chemistry and Polymer Technology, Polymer Research Center, Basrah University, Basrah, Iraq*
[c]*Department of Physics, College of Education for Pure Sciences, University of Basrah, Basrah, Iraq*
[d]*General Directorate of Education in Al-Muthanna Governorate, Ministry of Education, Al-Muthanna, Iraq*
e-mail: hussain_badran@yahoo.com
Received March 11, 2024; revised May 22, 2024; accepted May 22, 2024

Abstract—The current work presents the fabrication of polyaniline (PAni)/polyvinyl alcohol (PVA) nanofiber composites through electrospinning. The morphological properties of the sample evaluated by employing the field emission scanning electron microscope (FESEM) and the diameters of the samples are between 141 to 234 nm. The presence of both PVA and PAni in the nanofiber structure was evaluated with the aid of Fourier-Transformation Infrared Spectroscopy (FTIR). When a rifampicin-doped PVA film and a rifampicin-doped nanofiber PAni/PVA film were irradiated with a continuous wave laser beam at a wavelength of 532 nm, diffraction ring patterns (DFRPs) were seen. The nonlinear refractive index (NLDX) n_2, was determined from the number of observed rings. Large value obtained of the order of 212.48×10^{-8} cm^2/W for PAni/PVA nanofiber composites. The change in the nonlinear refractive index Δn, depends primarily on both the natural refractive index of the material and the NLDX, in which diffraction patterns play a major role in this change. In addition to that, the optical limiting) OPT (qualities were investigated. Within a solid PAni/PVA host, the dye shows of some impressive optical limiting features. It has been discovered that the mechanism responsible for the limitation of optical sensitivity is mostly of a thermal nature.

INTRODUCTION

In recent years, a variety of processing techniques have been explored to manufacture conducting polymer and nanofiber materials [1]. The potential for conducting fibers is huge as more electronic devices can be incorporated with textile fibers. The term "smart textile" refers to conducting fibers, where the possible applications could be toward medical, sensor, communication, and military applications. The current processing techniques include phase separation, hard templates, self-assembly, soft templates, interfacial polymerization, seeding, rapidly mixing, and electrospinning method [2–4].

The electrospinning technique is found to be the most efficient method for producing suitable polymer nanofiber textile materials with good fiber diameter ranges of 500 nm to 5 μm [5]. These fiber ranges of 500 nm to 5 μm have a large surface-to-volume ratio and are even potential for cell separation or membrane applications [6].

The electrospinning technique starts with an electrohydrodynamic process where a liquid droplet is electrified to generate a stream jet, followed by stretching and elongation of fibers. The parametric conditions such as flow rate and tips-to-collector distance will significantly alter the nanofiber textile quality [7]. In general, the main parameters to be controlled in producing high quality nanofibers include types of polymers, surface tension of the liquid droplets, polymer and composite material concentrations and solution properties including viscosity, polarity and conductivity [8]. Further adjustments in refining electrospinning conditions include tips-to-collector distance, applied external voltage and droplet flow rate [9].

The continuous nanofiber textile production of conducting Polyaniline through aqueous solution using electrospinning was formerly considered impossible because of the higher repulsive force between inorganic groups and their capability to form intermolecular interactions [10, 11]. PAni is regarded as one of the most extensively studied conducting polymers owing to its easy synthesis process and higher electrical conductivity [12, 13]. A new strategy for tuning PAni physical and chemical properties is through the incorporation of doping materials. PAni can be doped with

organic or inorganic dopants to increase its physical, chemical and mechanical properties [14]. The non-organic polymers that are capable in aiding the electrospinning includes polyvinyl pyrrolidone (PVP), polylactide (PLA), polyvinyl alcohol (PVA) and polyethylene oxide (PEO) [15, 16]. Among these polymers, PVA is considered to be the best platform in host polyaniline matrix due to its higher heat resistance, wider surface area, thermoplasticity, low toxicity and dimensional ability [17, 18]. Polymer materials have been used in the manufacture of vision devices, all optical switching devise and high resolution LCD. One of these materials is PAni/PVA nanofiber composite in order to protect these manufactured optical systems, as well as the human eye, from the effects of high-intensity light or laser light are debilitating, and the intensity of the incoming laser light It should be reduced in time [12]. OPT and self-diffraction are viable solutions for protective sensors and optical devices that use PAni/PVA nanofiber composite. These limiters device ensure that the filtering action is initiated instantly by the bright light in the inbox. In this instance, it modifies the absorptive and refractive characteristics of the materials that are enclosed within it, according to the bright light that is coming in to achieve a significant reduction in the transmission intensity that is the end outcome. When exposed to mild light, optical identifiers based on reverse saturable absorption (RESA) are extremely transparent, but when exposed to intense light, they become opaque. A further point to consider is that even if just RESA takes place, the quality of vision can still be maintained during the optical limit (OL) operation. After a certain threshold value, the samples begin defocusing the beam, which results in a bigger portion of the beam cross-section being cut off by the aperture. This causes the output power to initially increase in response to an increase in the input power for all samples. Therefore, the transmittance that was recorded by the photodetector stayed relatively constant, exhibiting a plateau region. Furthermore, the transmittance is saturated at a point that is described as the limiting amplitude, which describes the highest output intensity. This demonstrates that the limiting property is evident. In the current work, PVA and PAni/PVA nanofiber composites were prepared through electrospinning method and the result were thoroughly evaluated by using FTIR spectroscopy, X-ray diffraction spectroscopy, field emission scanning electron microscope (FESEM) and UV–Vis spectroscopy. The image-J computer software was further employed to determine the diameter of the synthesized nanofiber composite material. Measurements of DFRPs were carried out independently in order to quantify the nonlinear response of the device to the low power visible continuous-wave laser beam. The NLDX of the PVA film and the nanofiber film is computed, together with the overall change in their respective refractive indices. A comparison of the two films' OPT properties has been conducted.

EXPERIMENTAL

Preparation of Electrospinning Solution

The spinning solution was prepared by dissolving PVA (10% wt/vol) in distilled water at 50°C with continuous stirring overnight to obtain PVA aqueous solution. In a separate container of 15% wt/vol of the prepared PAni solution were dispersed into 15 mL of dimethyl sulfoxide (DMSO) solvent. The homogenized mixture of PAni and DMSO were carefully transferred into the prepared PVA. PAni/PVA nanocomposites were synthesized by blending PAni. This nanocomposites solution were further used in the produce of nanofiber textile materials.

Nanofiber Production Using Electrospinning Techniques

The electrospinning setup is used in the preparation of PAni/PVA textile composite nanofibers. The PAni/PVA composites solutions (10 mL) were filled in the syringe. The solution was pumped through the needle in the electrospinning setup. This is majorly to ensure the flow rate of the polymer melt solution is in constant motion. The electrospinning machine was linked to the higher DC voltage. The nanofibers composites PAni/PVA were obtained using an applied voltage 16 kV, flow rates of 0.45 mL/h and spinning distance 15 cm. The interval between the tips and the collector is considered the electrospinning distance. The electrospun nanofiber textile materials produced were collected on the detector, which was wrapped with aluminum foil. The electrospun nanofibers textile materials were left to dry under vacuum to remove residual solvent, as illustrated in Fig. 1.

Characterization

The PAni/PVA and PVA nanofibers textiles crystal structure was investigated using Bruker (D8 FOCUS), X-ray diffraction pattern (XRD) with CuK_α, and λ radiation wavelength. The chemical bonding presence in the PAni/PVA and PVA nanofibers textile were analyzed by Fourier Transformation Infrared Spectra (FTIR). The PAni/PVA's absorption spectral analysis and PVA nanofibers textile were further study by means of Ultraviolent UV–Visible (UV–Vis). Furthermore, the morphological properties of PAni/PVA and PVA nanofibers textile composites was analyzed by using field emission scanning electron microscopy ESEM (XL-30). The image-J was employed to study the average diameter of the PAni/PVA and polyvinyl alcohol nanofiber mixtures materials.
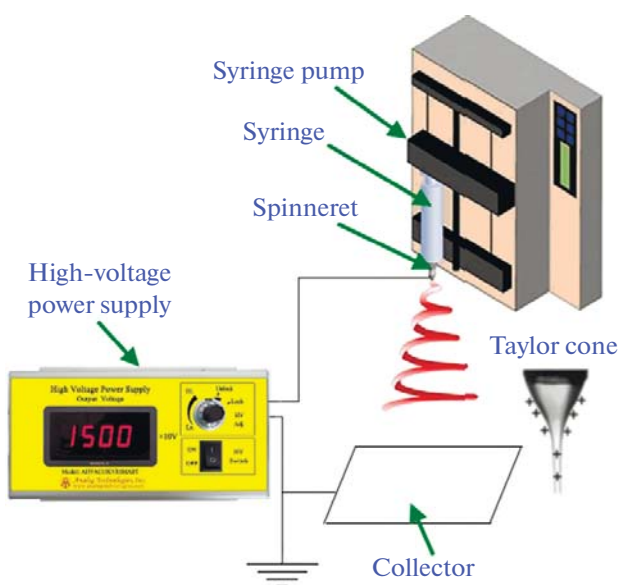
Fig. 1. Schematic representation of an electrospinning system.

RESULTS AND DISCUSSION

XRD Analysis of Composites

It was observed that most polymeric materials are not completely crystalline due to their chain arrangement, which indicates that the polymers have both crystalline and amorphous phases [19]. The presence of an amorphous phase revealed the existence of characteristics of an amorphous pattern in several forms. The amorphous phase of PVA and the crystalline phase of PAni/PVA nanofiber composite textiles were studied using deviation from x-ray spectrum analysis (XRD) the outcomes were revealed in Fig. 2.

Furthermore, Fig. 1 indicates the presence of PAni/PVA and PVA composite nanofiber materials on X-ray diffractometry ranging from $10°-90°$. The structural phase was found to match the joint committee on powder deviation standards file (JCPDS: 97-5869) to the phase pattern shown on each nanofiber composite material. Furthermore, the XRD pattern of PAni/PVA and polyvinyl alcohol nanofiber mixture materials contains a crystalline amorphous phase pattern with certain peaks appearing at $2\theta = 23.12°$, $24.14°$, $32.13°$, $37.14°$, $41°$, $43°$, $53.3°$, $57.42°$, $64.3°$, $65.4°$, $73.1°$, and $79.8°$ assigned to (101), (110), (311), (202), (302), (222), (122), (331), (112), (401), (501), (411), (143), and (201) which indicate the presence of PAni phase. Nevertheless, the peaks appear at $24.14°$, which is perpendicular to the PAni matrix and ascribed to the parallel periodicity [20].

FTIR Analysis of Composites

The FTIR spectra are far one of the major investigative techniques used to study the chemical bonding analysis of materials. However, these instruments were utilized to analyze the prepared PVA and PAni/PVA nanofiber composite materials as well as determine the presence of functional groups in the polymer materials. Figure 3 revealed the FTIR spectra of the synthesized polyvinyl alcohol and polyaniline/polyvinyl alcohol nanofiber compounds electrospun at certain parameter, which include high DC applied voltage tips to collector distance and flow rate, respectively. However, the weak intensity peaks were demonstrated at 2918, 2942, 3284, and 3299 cm^{-1} assigned for vibrating and stretching of the O−H group found in the polyvinyl alcohol nanofibers materials and vibration stretching of the amine group found in mixture materials of PAni/PVA nanofibers, as shown in Fig. 2.
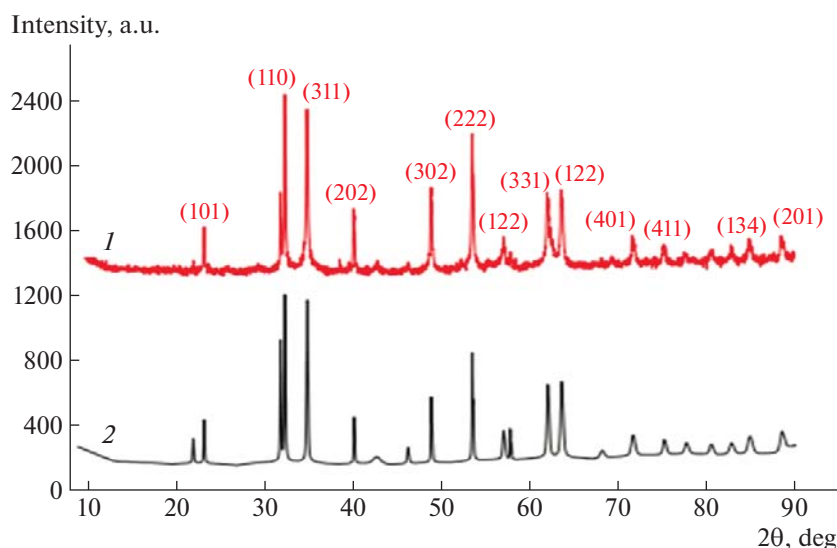

Fig. 2. XRD of (*1*) PVA nanofibers and (*2*) PAni/PVA nanofiber composite.
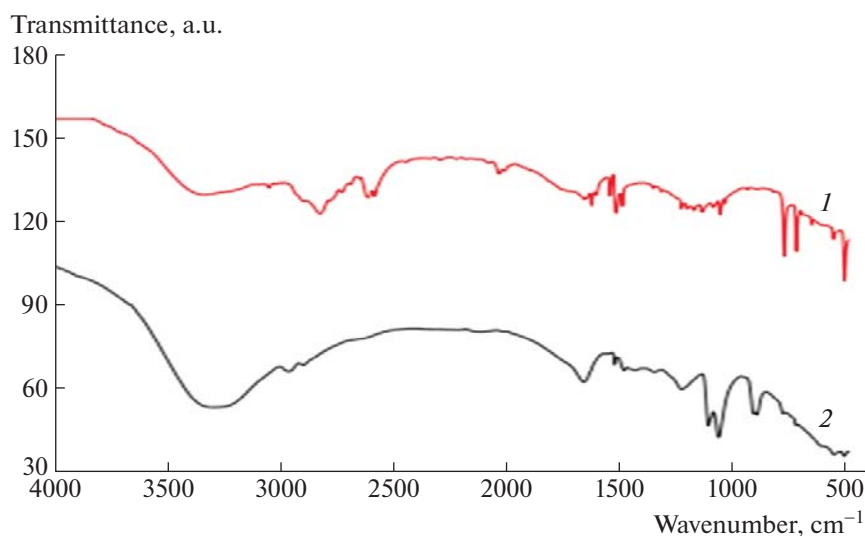
Transmittance, a.u.

Fig. 3. FTIR spectrum of (*1*) PVA nanofibers and (*2*) PAni/PVA nanofiber composite.

The bands that can be seen in the FTIR spectrum of the generated PAni/PVA nanofiber composites at wavelengths ranging from 1000 to 1656 cm^{-1}, together with certain weak linkages for PVA nanofiber materials from 3000 to 1450 cm^{-1}, are in fact caused by the presence of alkane and amine groups [17, 18]. Additionally, the peaks appearing at 1401 to 1000 cm^{-1} indicated that C=O vibrating stretching and C−O symmetry within the nanofiber composite materials. Some peaks were further revealed at 581 cm^{-1} in the FTIR spectra of the prepared nanofiber composites, these bonds are assigned to stretching vibrations of the C−H group that are usually present in the PAni and PVA nanomaterials [19, 20]. Several vibrating bonds were found ranging from 1401−847 cm^{-1} which might correspond to the CH$_3$ group stretching vibration that exists in the PAni and PVA nanotubes, this can simply reveal the absence of H$_2$O molecules in the composites [21].

UV−Visible Analysis of Composites

In the current research, UV−Visible spectroscopy was used to study the optical absorption analysis of the prepared PVA and PAni/PVA nanofiber composite materials. The optical absorption spectroscopy result was recorded in the range of 250−900 nm wavelength through Shimadzu UV-1800 spectroscopy. However, the UV−Vis spectrum of the prepared PVA and PAni/PVA nanofiber composites electrospun at some parameters that include high DC voltage, tip to collector distance, and flow rate revealed the fabricated nanofiber result in the Fig. 4. The more intense bond found at 670 nm corresponds to π−π* benzonoid ring transition. This shoulder-like structure revealed the

peaks at 400−700 nm presence of emeraldine salt phase of the doped PAni and PVA in the composite materials [22, 23].

Generally, the nanofiber composite materials with a certain quantity of polyaniline revealed nearly the same peaks in the resulting UV−Vis spectra at 400−700 nm [24]. This indeed is attributed to the higher component of PVA within the nanofiber composite materials and the interaction of photons of light with conducting electrons in the PAni matrix, which result in the high absorption, however the nanofiber composites are quite transparent in the visible region [25]. The structure found in the resulting spectra of the nanofiber indicates very high absorption (400−700 nm).

Surface Morphology Study of PVA and PAni/PVA Nanofiber Composites

The electrospinning technique was employed in the fabrication of nanofiber composite materials. PVA was used to stabilize the formation of electrospinning solutions. Compared to other materials, it is low-cost nontoxic material that makes it easy to realize a good solution for electrospinning setup. The morphology of the synthesized PVA and PAni/PVA nanofiber mixtures were confirmed using the Field Emission Scanning Electron Microscope (FESEM), and the result was revealed in Fig. 5. As usual the polyvinyl alcohol, as well as PAni/PVA nanofiber mixtures, were achieved after loading 10 mL rotation solution and electrospun at 16 kV. Homogeneous nanofibers with a large diameter and a smooth surface were obtained in PVA nanofiber materials when the incorporation of PAni with PVA solution led to a depletion in the diam-
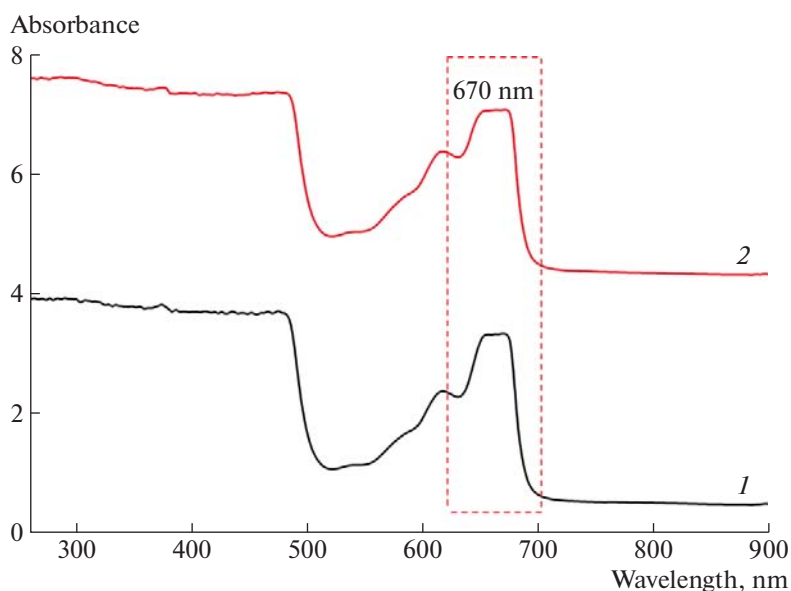
Fig. 4. UV–Vis spactra of (*1*) PVA nanofibers and (*2*) PAni/PVA nanofiber composite.
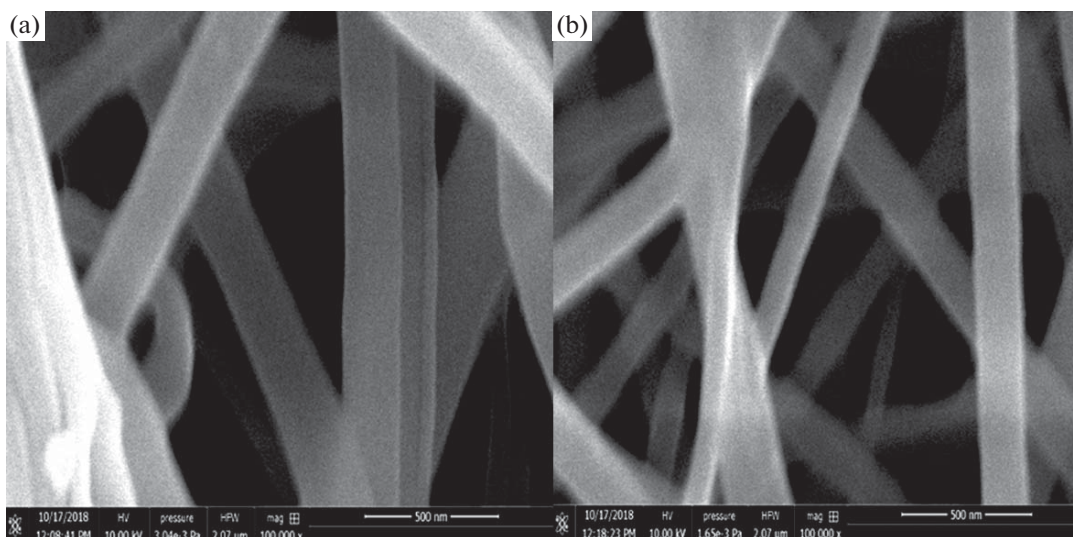

Fig. 5. FESEM analysis of (a) PVA nanofibers and (b) PAni/PVA nanofibers composites spun at 16 kV, 15 cm tips to collector distance and 0.45 mL/h.

eter of the nanofiber textile. This is in line with the finding from literature [26, 27] as shown in Fig. 5.

The addition of PAni into PVA nanotubes causes the net electric charge density in the solution to increase, indicating the production of nanofiber with a smaller diameter [28, 29]. The PAni existence in the mixture solution shows the correlation of the addition of salts to the electrospinning solution. The addition PAni not only alters the viscosity of the solution but also increases the dielectric constant as well as the electrical conductivity concerning the spinning solution, favoring the nanofiber production with a smaller

diameter, as shown in Fig. 6. In addition, image-J computer software was employed to approximate the diameter of polyvinyl alcohol and polyaniline/polyvinyl alcohol nanofiber mixtures materials the results was revealed in Fig. 6. It was found from image-J result that the diameter of PVA nanofiber was found to be averagely to be 234 nm. Although, presence of PAni in the composites reduce the diameter, as a result the diameter of PAni/PVA nanofiber composites was exhibited at 141 nm that is completely less than unmixed PVA nanofiber, suggesting that addition of
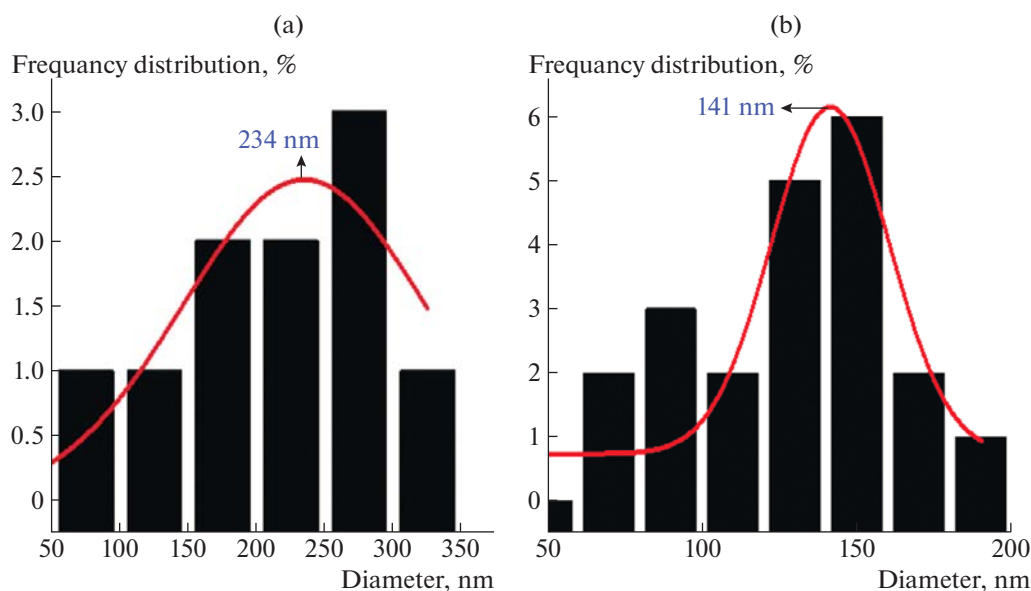
(a)

Frequancy distribution, %

234 nm

Diameter, nm

(b)

Frequancy distribution, %

141 nm

Diameter, nm

Fig. 6. Diameter distribution of (a) PVA nanofiber and (b) PAni/PVA nanofibers composites.

PAni to PVA lower the diameter of the nanofiber materials [30, 31].

Comparative Study

When it comes to electrospinning, surface tension is extremely important because if it is too high, it might cause the PAni/PVA nanofiber to deform into droplets. With the use of electric fields, this problem may be solved by forming polymer solution jets. For beads, a high surface tension is advantageous, which results in reduced surface energy. As a result of their low conductivity and high surface tension values, many solvents have the potential to influence the production of electrospun. Additionally, flow rate, surface tension, the rotational parameter of the applied voltage, the distance between the tip and collector, and other factors differ among different polymers. The variation of spinning parameters is illustrated in Table 1. The distance between the tip and collector, the applied voltage (which ranges from 7 to 25 kV), and the flow rate (which varies from 0.0025 mL/min to 0.5 mL/h) all contribute to the fibre synthesis process. Voltage increase may result in the formation of beads or a reduction in fibre diameter. The optimum distance is 15 cm; increasing the range from 15 to 25 cm maximizes bead formation.

Nonlinear Experimental

Nonlinear film preparation. The dye rifampicin was dissolved in *N*-methyl-2-pyrrolidone as a solution sample (NMPD). The rifampicin solution has concentrations of 0.50 and 0.65 mM. Since it is stiff and rigid, PAni/PVA nanofiber was chosen as the host material for the solid films. After dissolving a known amount of PAni/PVA nanofiber and Rifampicin in NMPD separately (the concentration of rifampicin in NMPD is 0.5 mM), the two solutions were blended and agitated for 3 hours with a magnetic stirrer. PAni/PVA nanofiber solution and rifampicin solution were mixed in a 1 : 1 ratio. The film sample was made using the casting procedure on a glass stratum slide and dried at 35°C for 24 hr. A digital micrometer to calculate the thickness of the sample and is found to be 7 μm. Similarly, the other film was prepared for the rifampicin doped PAni/PVA nanofiber with a concentration of, 0.65 mM. The thickness of the film was found to be equal to 9 μm.

The absorption spectra of the rifampicin doped PVA and rifampicin doped PAni/PVA nanofiber with different concentrations are shown in Fig. 7. From Fig. 7, it is indicated that the increase in the number of particles per unit volume [42] due to the difference in concentration increases the absorption spectra of the sample (PVA film and PAni/PVA nanofiber film). The absorption coefficients α_{coff} for each sample were determined in the spectral range of 300−650 nm by the analysis of the optical absorbance spectra from the following relationship [43–45].

$$\alpha_{coff} = \frac{2.303 A_{abs}}{T_{th}}, \quad (1)$$

where A_{abs} and T_{th} are the absorbance and thickness of the sample. At 532 nm wavelength the value of the absorption coefficient α_{coff} of the rifampicin doped PVA and rifampicin doped PAni/PVA nanofiber were calculated and they are given in Table 1. It can be observed that high values of absorption coefficients

Table 1. The parameters of electrospinning utilized in the production of diverse assortments of electrospun nanofibers

Electrospun sample	Diameter, nm	Voltage, kV	Flow rate, mL/h	Distance, cm	Reference
PAni/PVA nanofibers composites	141	16	0.45	15	Present study
PVA nanofiber	234	16	0.45	15	Present study
Polyvinylidene fluoride (PVDF)	500	25	0.5	15	32
Zinc oxide-polyvinylpyrrolidone (ZnO/PVP)	3−150	7	0.3	5	33
Polyvinyl alcohol (PVA)/gold NPs	200	9	1.5	17	34
PVDF /Lithium chloride	−	20	0.3	20	35
Polymethylmethacrylate (PMMA)/silver NPs	318.5 ± 24.9	20	1.5	20	36
p-Hydroxybenzoic acid (PHBA)	270−520	13	1	12	37
PVDF/p-hydroxybenzoic acid	150	25	−	15	38
Calcium/curcumin	104	20		15	39
Polyethylene oxide (PEO)	10−1000	7−8	0.0025	15	40
PVDF/barium titanate	110	18	0.12	15	41

suggest a high possibility of electronic transitions, which then results in direct transitions. This is because direct transitions are the consequence of the chain reaction that begins with electronic transitions [46−48].

Self diffraction technique. A self-diffraction ring pattern can be seen in the far field when a Gaussian distribution lights a nonlinear material sample. Figure 8 shows the experimental setup for the observed self-diffraction ring pattern. A glass-positive 5 cm focal length lens, a digital photographic CCD camera, and a standard CW laser (type SDL-532-100T) working on the lowest fundamental spatial distribution TEM_{00} mode, generating green light (532 nm, 40 mW) were employed. A coherent multi-wavelength power meter was used to measure the laser output power.

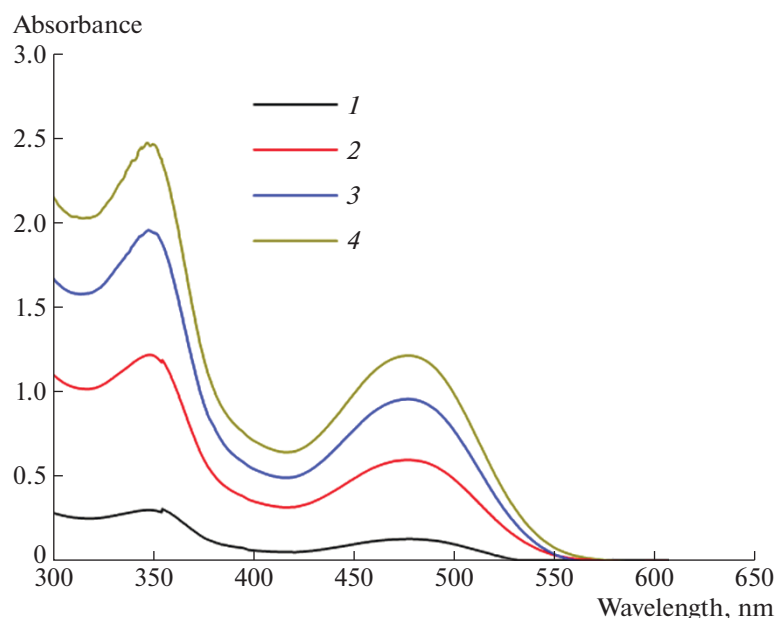The self-diffraction ring patterns were casted on a semi-transparent screen measuring 30×60 cm. The

Fig. 7. Absorption spectra for (*1*) 0.5 mM-PVA film, (*2*) 0.65 mM-PVA film, and (*3*) 0.5 mM PAni/PVA nanofiber composites film, (*4*) 0.5 mM PAni/PVA nanofiber composites film.
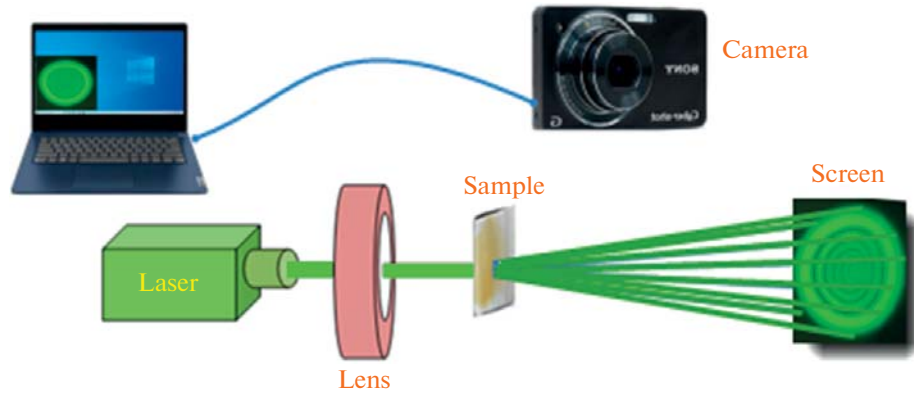
Fig. 8. Experiment setup for measuring diffraction rings.

laser beam waist ω_0 at the focus can be calculated using the relationship [49, 50]:

$$\omega = 1.22 f \lambda / \omega_0, \qquad (2)$$

ω_0 is the radius of the laser beam as it left the output CW coupler of the laser. The beam radius impacting the nonlinear sample depends on the laser light wavelength λ according to Eq. (2) so that for $f = +50$ cm, and $\omega_0 = 1.2$ mm (at $1/e^2$), $\omega = 27.043$ μm. To meet the nonlinear thin medium criteria, the sample thickness T_{th} must be lower than the Rayleigh length, the Rayleigh length Z_R, can be estimated with the help of the relationship [51−53]:

$$Z_R = \pi \omega^2 / \lambda, \qquad (3)$$

where $\omega = \omega_{532}$ and the wave length, λ has the same definition so that $Z_R = 2.76$ mm, i.e., the sample thickness is satisfied ($T_{th} < Z_R$). The nonlinear refractive index can be calculated using the number of diffraction rings that appear on the screen. The change in the phase can be written as [54−57].

$$\Delta \Phi = \Delta n k T_{th}, \qquad (4)$$

where $k = 2\pi/\lambda$ is the beam wave vector in a vacuum. The relation between $\Delta \Phi$ and the number of rings, N can be written as [58−62]:

$$\Delta \Phi = 2\pi N. \qquad (5)$$

The equation for the linear and nonlinear refraction coefficients is [63−66]:

$$n = n_\circ + n_2 I, \qquad (6)$$

where n is the total refractive index. The total change in refractive index can be written as [67−71]:

$$n = n_\circ + \Delta n \quad \text{and} \quad \Delta n = n_2 I, \qquad (7)$$

Using Eqs. (2)−(7), the magnitudes of nonlinear n_2, Δn, and $\Delta \Phi$ are shown in Table 2.

Figure 9 explains the far field DFRPs of the rifampicin doped PVA film and the rifampicin PAni/PVA nanofiber composite film with different concentrations. It is evident that when the film concentrations rise, the number of diffraction rings rises as well.

The results in Table 2 represent the investigation data for the nonlinear refractive index and the number of self diffraction patterns with PVA film and nanofiber film. It can be seen from Table 2 that dye doped PAni/PVA nanofiber composite films play a fundamental role in improving their nonlinear optical properties. When the dye doped pure PVA film is illuminated with a laser at an intensity of 3.483 kW/cm^2, it exhibits nonlinear properties represented by the number of rings whose magnitude is 2 rings on the screen. For the same incident intensity from a CW laser, when dye doped pure PVA film with a concentration of 0.65 mM, the sample showed 4 rings on the screen and the value of the nonlinear refractive index was equal to 1.23×10^{-8} cm^2/W. But when the amount of concen-

Table 2. The nonlinear optical parameters

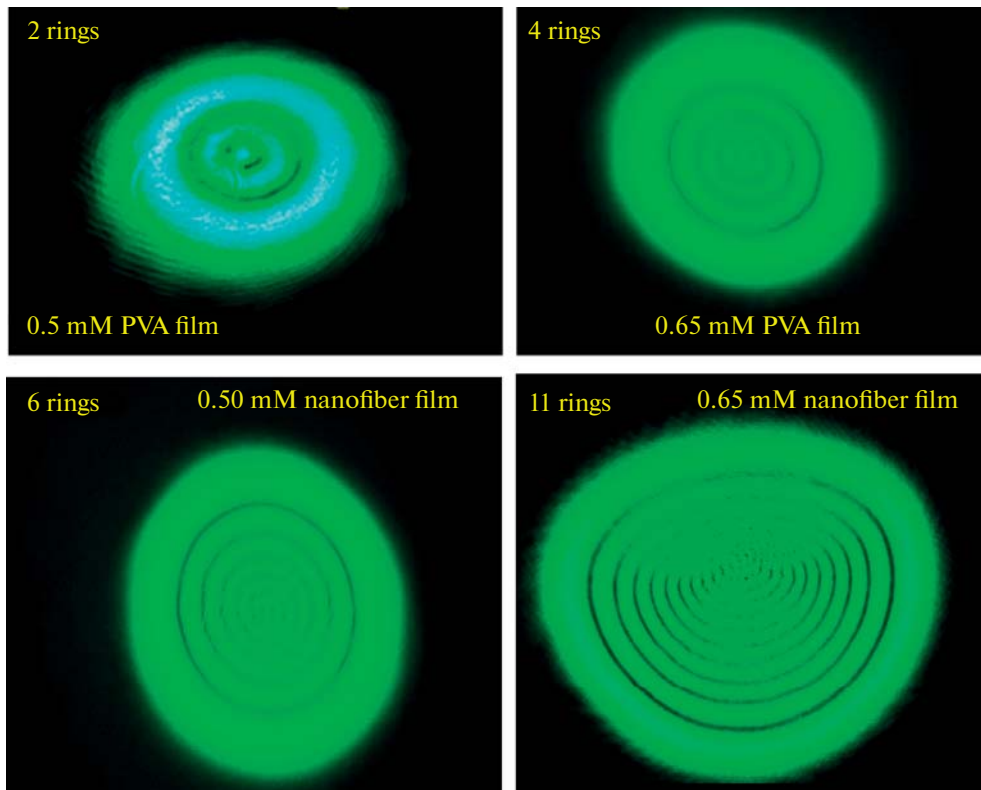| Sample	Rings no.	α_{coff}, cm^{-1}	$\Delta \Phi$	$n_2 \times 10^{-8}$, cm^2/W	$\Delta n \times 10^{-4}$
PVA-0.5 mM film	2	1.01	0.219	0.53	0.18
PVA-0.65 mM film	4	3.08	0.438	1.23	0.43
Nanofiber 0.5 mM film	6	666.29	0.657	106.49	37.10
Nanofiber 0.65 mM film	11	725.11	1.205	212.48	74.02

Fig. 9. The far-field DFRPs observed for rifampicin doped PVA film and rifampicin dye doped PAni/PVA nanofiber composites film, with different concentration (a) 2, (b) 4, (c) 6, and (d) 11 rings.

tration is large and within 0.5 mM and 0.65 mM (nanofiber composite films) the number of rings shown on the screen is equal to 6 rings and 11 rings and the values of the nonlinear refractive index are within 106.49×10^{-8} and 212.48×10^{-8} cm^2/W respectively. Increasing the concentration of the sample will increase the aggregation of the rifampicin dye molecules in a nonlinear sample at the concentration point of the higher concentration, which in turn increases the number of self- diffraction ring patterns and the size of the outer patterns. The beam profile distribution was carried out using Thorlabs Beam BP209. The Gaussian profile distribution data for rifampicin doped PVA film and rifampicin doped nanofiber composite film is shown in Fig. 10.

All of the Thorlab graphs show the typical structure of the patterns, where the spherical nature of the distribution is obvious, with no major differences in the surface before and after doping. The temperature gradient in the upper half of the hot zone owing to convection is aided by thermal upward currents caused by gravity attraction. The reduction in the refractive index gradient, which diminishes the phase modulated optical field in the upper half of the laser beam, is responsible for this phenomenon [72]. Figure 11 shows how external yaw is minimized in that location, causing the pattern to seem compressed from above.

Because of the short time it takes for energy to pass from the laser beam to the nonlinear sample, the local temperature of the medium rises. The spatial distribution in the nonlinear sample differs greatly from the applied basic TEMoo Gaussian laser intensity due to heat transfer, conduction, and convection. Because the laser beam causes immediate heating of the sample, the system (medium) soon approaches a steady state. Figures 10 and 11 show that when the input power rises, the width of the outermost ring in the horizontal and vertical directions of the distant field grows for each nonlinear sample concentration. However, compared to the horizontal direction, the vertical ratio is lower (see Figs. 11 and 12).

When the PVA film and PAni/PVA nanofiber composite film were 1.5 cm before the lens focal point, i.e., convergent wave front, and the sample was 1.5 cm after the focal point, i.e., divergent wave front, two different types of DFRPs resulted. This demonstrates that the interaction between the polymer film and the laser beam is dependent on the wave front type of the laser beam. This can be seen in Fig. 13.

Optical Limiting

The optical limiter is a device that is used to weaken high-power laser beams and let low-power laser beams
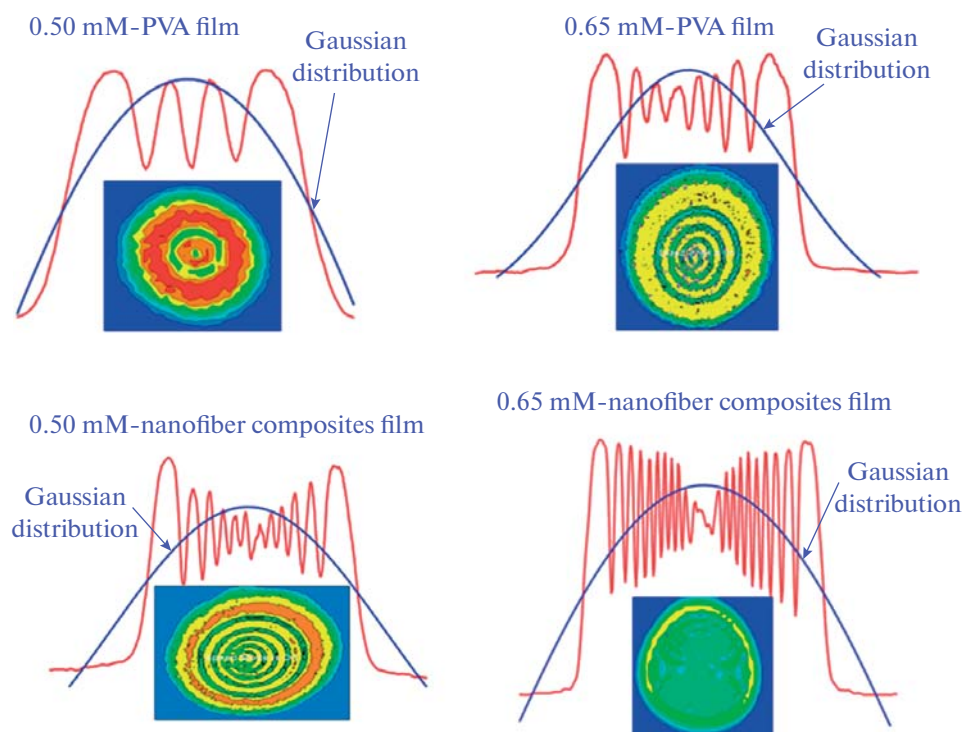
Fig. 10. Beam profile distribution of the PVA film and nanofiber composites film.
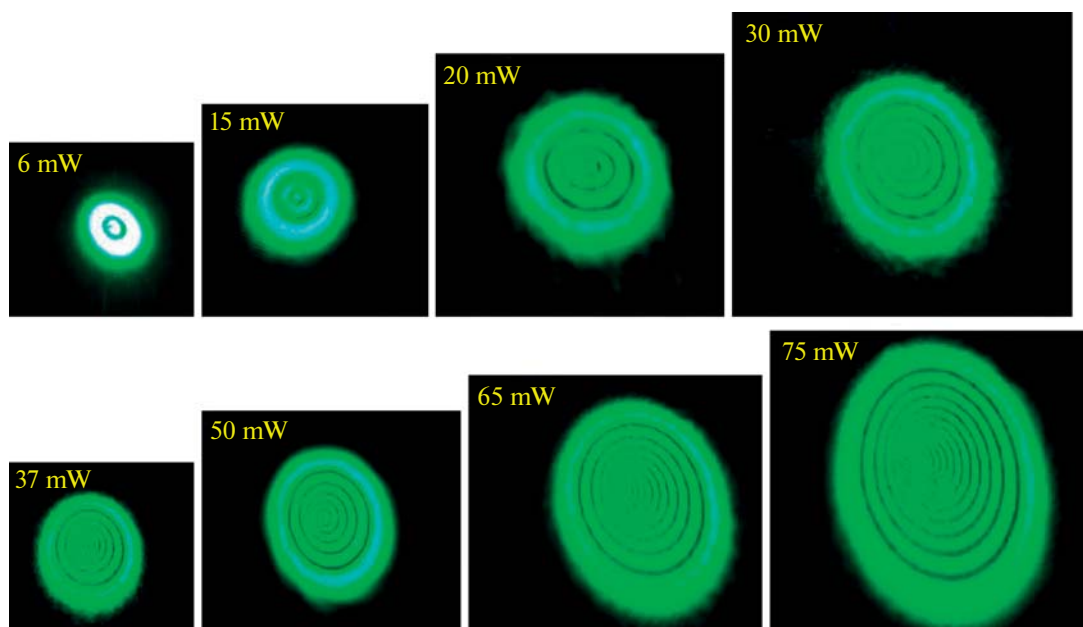

Fig. 11. Experimentally ring patterns with different input power in the 0.65 mM nanofiber composites film.

through. The optical limiting threshold (OPT$_{th}$) value is the most essential parameter in this device since it defines the efficiency of any material and whether or not it can be utilized as an optical limiter. This device is used to restrict the amount of light that can pass through it. In this part of the article, the OPT features of the rifampicin : PVA film and the rifampicin : PAni/PVA nanofiber film are investigated. The threshold values are calculated, and they are compared with those of other materials that are already on

the market and are known as optical limiters. The acquired results of the OPT characteristics of the rifampicin : PVA film and the rifampicin : PAni/PVA nanofiber film are presented in Fig. 14.

These findings were achieved by using the setup shown in Fig. 8 and making the changes stated in section 7.2. At low input power, the relationship between input power and output power is linear, which means that the samples let the laser beam through. As the input power increased, the relationship between input power and output power became irregular, and then the output power became steady. Calculating the value of the OPT_{th} is necessary, as was previously described, in order to determine how effective the material is at acting as an optical limiter and quantify its effectiveness. This threshold value is the input power required to reduce the transmittance through the medium by half of what it was before. Figure 15 depicts the result of plotting the normalized transmittance as a function of the input power in order to determine the OPT_{th} value. The specific features of the OPT behavior observed as follows, this demonstrates that PVA and nanofiber composite films are good candidates for use as optical limiting. The nanofiber composite film exhibits distinctive and impressive optical limit behavior, which is represented by an amplitude of 3.8 mW for the rifampicin : PAni/PVA nanofiber film and a value of about 5.4 mW for the PVA film. While the saturation point is 4.2 mW for the rifampicin : PAni/PVA nanofiber film and 5.8 mW for the PVA polymer, This indicates that the rifampicin dye has enhanced optical limiting properties in a good and striking way. This demonstrates that PVA and nanofiber composite films are good candidates for use as optical limiting. The threshold values of nanofiber film and PVA film, 8.01
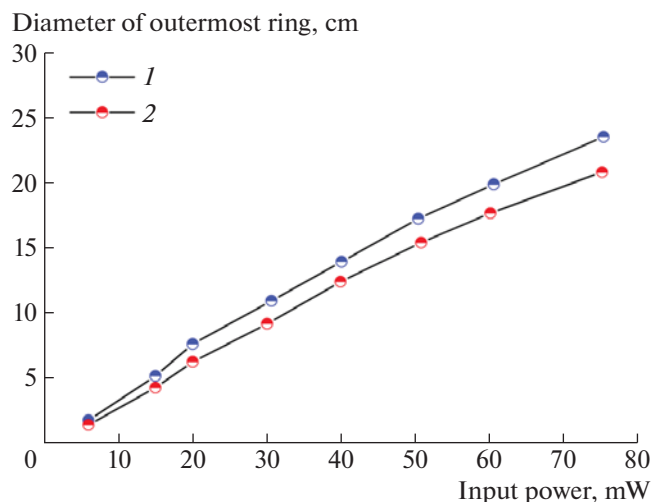
Diameter of outermost ring, cm

Fig. 12. (*1*) Horizontal and (*2*) vertical outermost ring diameters for 0.65mM nanofiber composites film.

and 13.76 mW respectively, are calculated from the curve in Fig. 15. It is noted that the threshold value of the nanofiber film is very low compared to the value obtained from the PVA film, which makes it a good material to be chosen as a promising material in optical limiter devices.

There are now a lot of materials that have been shown to be useful as optical limiters because of the low threshold values that they have. Some examples of these materials are listed in Table 3. When contrasted with the threshold values of these other materials, the rifampicin doped PVA film and the rifampicin doped PAni/PVA film (nanofiber composite film) have the

Table 3. Comparison between the threshold value of PVA film and nanofiber composite film and those of some materials that are known as visual limiters

| Samples	OPT_{th}, mW	References
Rifampicin : PAni/PVA nanofiber composite film	8.01	Present work
Rifampicin : PVA film	13.76	Present work
ZnS-Nanoparticle film	9.7	73
CdS-Nanoparticle film	14.6	74
$ZnO-5TiO_2$ nanocomposite	13	75
Nanocomposite gold nanoparticles/epoxy resin	66	76
Oligothiophene-doped liquid crystals	25	77
Copper phthalocyanine doped PHPP	10.9	44
Organic compound doped polyO-methoxyaniline (POMA)	12.44	49
Virgin avocado oil (VAVO)	12	78
Platinum nanoparticles	30 ± 2	79
Leishman dye doped PMMA	10.4	80
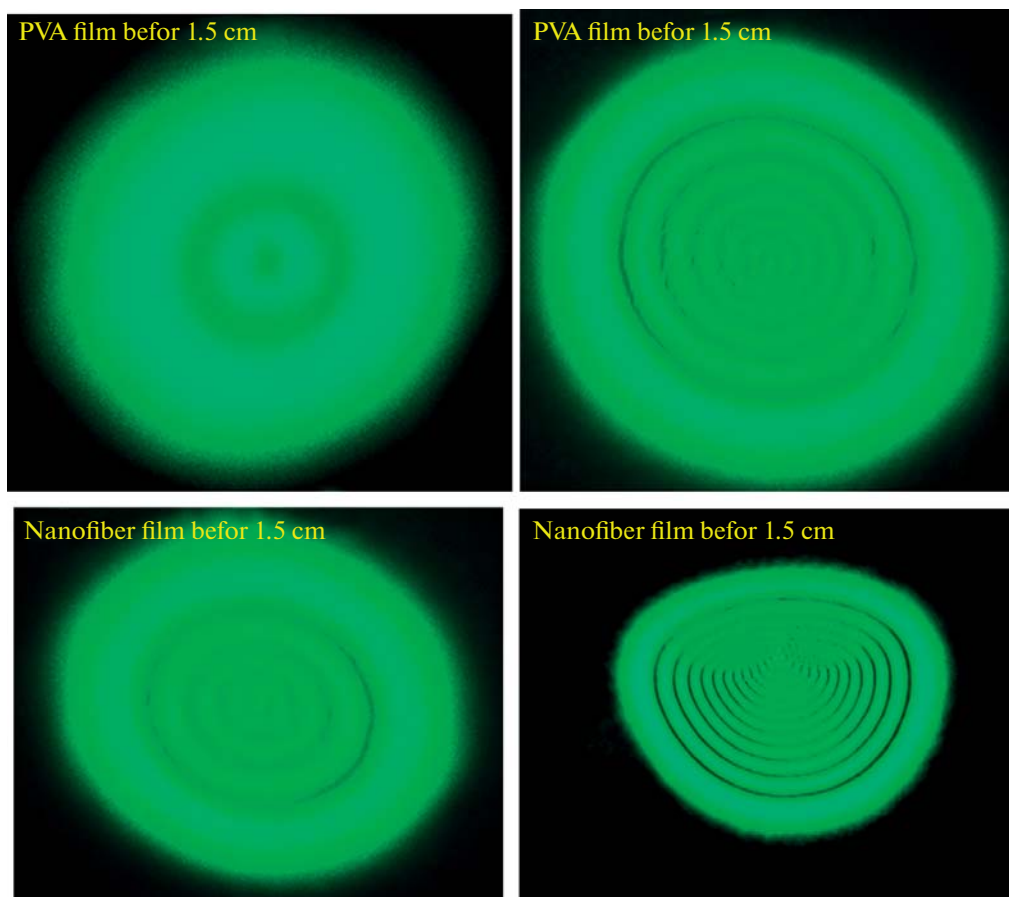
Fig. 13. DFRP intensity when the input power is 55 MW and the film is 1.5 cm before and after the lens focus point in PVA and nanofiber composite films.

lowest threshold values. This demonstrates that the PVA film and the nanofiber composite film are good candidates for use as optical limiters.
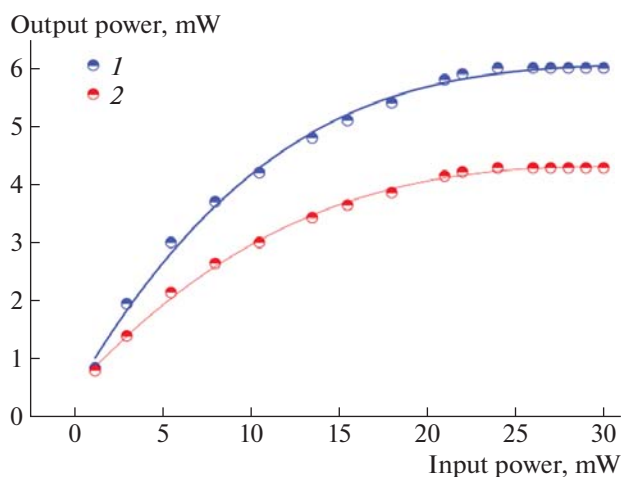

Fig. 14. Limiting behavior carve for (*1*) PVA film and (*2*) nanofiber film.

CONCLUSIONS

In summary, the structural pattern of the PVA and PAni/PVA nanofiber composites was investigated using XRD, and the crystalline phase was recorded on the diffractometer at 20° to 90°. The X-ray diffraction (XRD) pattern of PVA and PAni/PVA nanofiber materials shows the characteristic behavior of both amorphous and crystalline phases by indicating the peaks at $2\theta = 23.12°$ and $24.14°$ in the prepared materials. The FTIR analysis is used to study the functional group of the prepared materials. Findings show that several vibrating bonds were found, which could correspond to the stretching vibration of the methyl group appearing in the polyaniline and polyvinyl alcohol nanotubes. This can simply reveal the absence of H_2O molecules in the composites. The bands appearing at 1000, 1334, 1401, 1416, 1606, and 1656 cm^{-1} in the whole FTIR spectrum of the prepared nanofiber composites are indeed because of the alkane and amine group vibrations stretching, which revealed the bond at 481, 592, and 847 cm^{-1}, which are oxygen derivatives, carbon, and hydrogen vibrating stretching. The morphology of the prepared PVA and PAni/PVA
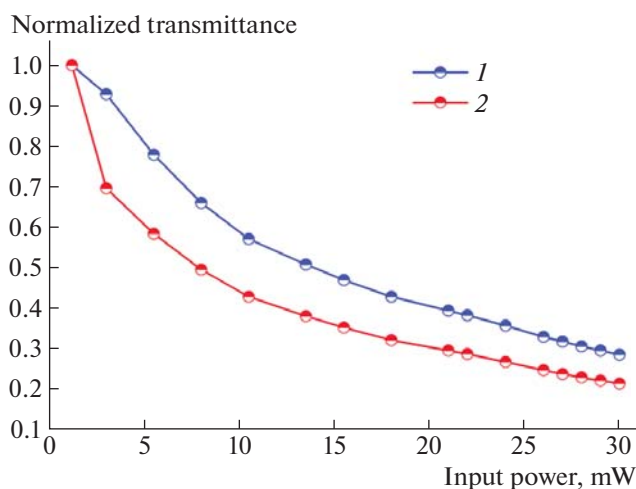
Normalized transmittance

Fig. 15. Normalized transmittance curve for (*1*) PVA film and (*2*) nanofiber film.

nanofiber composites was investigated using FESEM, and it was observed that with the addition of PAni to PVA nanotubes, the net electric charge density in the solution increased, which led to the production of nanofibers with a smaller diameter. Furthermore, it was found from the image-J result that the average diameter of PVA nanofibers was 234 nm. Although the presence of PAni in the composites reduces the diameter, as a result, the diameter of PAni/PVA nanofiber composites was exhibited at 141 nm, which is completely less than unmixed PVA nanofiber, suggesting that the addition of PAni to PVA lowers the diameter of the nanofiber materials. Researchers looked into the linear and nonlinear behavior as well as OPT characteristics of rifampicin doped PVA film and rifampicin doped PAni/PVA film. The nonlinear measurements were carried out using methods for self-diffraction with continuous-wave (CW) laser light at 532 nm. It has been discovered that the host polymer film has a significant impact on the linear and nonlinear optical as well as the optical limiting parameters. According to the findings of the experiments, the rifampicin-doped PAni/PVA film (also known as a nanofiber composite film) demonstrates significant nonlinearities. All of these experimental findings demonstrated that the manufactured sample, which consisted of a nanofiber composite sheet, is a promising material for use in nonlinear device applications.

AUTHOR CONTRIBUTION

The present submissions represent original work. The current work is not considered for publication elsewhere in any other form. Also, all of the co-authors aware of this submission and they contributed to this work. **Rajaa M. Abdullah:** An individual who took part in the investigation of the PAni structure and the characteristics of nanofiber composites. **Mohammed T. Obeed:** Interpreted the data, revised the manuscript and Data curation. **Zainab J. Sweah:** Data analysis, interpretation, and revised manuscript. **Hussain A. Badran:** Served as a supervisor for the entirety of the study, participated in the revision of the article, drafted the first draft, developed the study, and carried out the majority of the experiments. **Riyadh Ch. Abul-Hail:** Data analysis, and carried out the majority of the experiments. **Maytham Qabel Hamzah:** Authored the article after doing the analysis of the results.

FUNDING

CONFLICT OF INTEREST

The authors of this work declare that they have no conflicts of interest.

REFERENCES

1. R. K. F. Al-Fahed, A. R. Alaa, S. M. Munaf, and A. B. Hussain, Polym. Sci., Ser. B **63**, 773 (2021).

2. B. Michal, M. Varga, P. Jan, A. Zhigunov, and J. Vohlídal, Eur. Polym. J. **49**, 3904 (2013).

3. Y. Yang, E. Liu, L. Li, Z. Huang, H. Shen, and X. Xian, J. Alloys Compd. **505**, 555 (2010).

4. X. Chao, X. Feng, W. Bin, and J. L. Tian, J. Nanomater. **2011**, 1 (2010).

5. S. Hosseini, P. Azari, E. Farahmand, S. N. Gan, H. A. Rothan, R. Yusof, L. H. Koole, I. Djordjevic, and F. Ibrahim, Biosensor. Bioelectron. **69**, 257 (2015).

6. M. Zuwei, K. Masaya, Y. Thomas, H. Wei, and R. Seeram, Biomaterials **26**, 2527 (2005).

7. C. J. Luo, D. S. Simeon, E. Stride, E. Pelan, and M. Edirisinghe, Chem. Soc. Rev. **41**, 4708 (2012).

8. M. Janja, B. Helena, Š. Zupančič, and J. Kristl, Polymers **11**, 692 (2019).

9. K. Saraswathi, M. S. B. Reddy, R. M. Muni, G. B. Rani, V. K. Rao, and K. S. Kishor, Macromol. Mater. Eng. **306**, 2100410 (2021).

10. S. Nagarajan, C. Pochat-Bohatier, S. Balme, P. Miele, S. N. Kalkura, and M. Bechelany, Pure Appl. Chem. **89**, 511 (2017).

11. E. Catalano and A. Di Benedetto, J. Phys. Conf. Ser. **841**, 1 (2017).

12. M. Beygisangchin, R. S. Abdul, S. Shafie, A. R. Sadrolhosseini, and H. N. Lim, Polymers **13**, 2003 (2021).

13. V. Sada, N. K. Bhajanthri, P. Bobbala, S. R. Yakkate, and V. V. J. Nimmagadda, Arab. J. Chem. **12**, 588 (2019).

14. G. Salimbeygi, K. Nasouri, A. M. Shoushtari, R. Malek, and F. Mazaheri, Micro Nano Lett. **8**, 455 (2013).

15. M. Mumtaz, C. Labrugère, E. Clouet, and H. Cramail, Langmuir **25**, 13569 (2009).

16. M. Shen, H. Cai, X. Wang, X. Cao, K. Li, S. H. Wang, R. Guo, L. Zheng, G. Zhang, and X. Shi, Nanotechnology **23**, 105601 (2012).

17. M. C. Zhang, B. H. Guo, and J. Xu, Crystals **7**, 1 (2016).

18. K. I. Ajeel and Q. S. Kareem, J. Phys.: Conf. Ser. **1234**, 012020 (2019).

19. G. Zhen, Y. Yunfei, Z. Jia, X. Yongyang, J. Min, C. Fei, Z. Hua, W. Ping, J. Honghua, and Y. Xiaoyu, Bioresour. Bioprocess **5**, 27 (2018).

20. M. Koosha and H. Mirzadeh, J. Biomed. Mater. Res., Part A **103**, 3081 (2015).

21. F. Liu, Q. N. Qing, and Y. Murakami, Text. Res. J. **83**, 510 (2013).

22. T. J. Alwan, Z. A. Toma, M. A. Kudhier, and K. M. Ziadan, Madridge J. Nanotechnol. Nanosci. **1**, 1 (2016).

23. Y. L. Hong, X. Lan, P. T. Xiao, and Q. S. Zhi, J. Text. Inst. **106**, 37 (2014).

24. O. M. Salim, M. H. Kasim, H. J. Abdullah, Q. H. Maytham, N. T. Alaa, M. S. Roslan, and A. A. Mohd, Int. J. Psychosoc. Rehabil. **24**, 4532 (2020).

25. H. Harsojo, A. F. Waluyo, H. Sosiati, and K. Triyana, Adv. Mater. Res. **1123**, 237 (2015).

26. O. M. Salim, M. Kasim, H. J. Abdallah, M. Q. Hamzah, N. T. Alaa, S. Sopi, and A. A. Mohd, Solid State Technol. **63**, 256 (2020).

27. A. Bouarissa, A. Gueddim, N. Bouarissa, and S. Djellali, Polym. Bull. **75**, 3023 (2018).

28. A. R. Saddam and F. E. Abbas, Mater. Today: Proced. **45**, 5819 (2021).

29. H. K. N. Nor, M. Y. Noordin, I. Ani, M. Effaliza, and K. Denni, Mater. Sci. Eng., C **70**, 520 (2017).

30. M. Na, W. Xiangqin, X. Binjie, C. Zhuoming, and L. Yan, Text. Res. J. **89**, 2490 (2019).

31. W. I. Singh, S. Sinha, N. A. Devi, S. Nongthombam, S. Laha, and B. P. Swain, Polym. Bull. **78**, 6613 (2021).

32. C. Ribeiro, D. M. Correia, I. Rodrigues, L. Guardao, S. Guimaraes, R. Soares, and S. M. Lanceros, Mater. Lett. **209**, 118 (2017).

33. J. A. Park, J. Moon, S. J. Lee, S. C. Lim, and T. Zyung, Curr. Appl. Phys. **9**, S210 (2009).

34. J. Wang, H. B. Yao, D. He, C. L. Zhang, and S. H. Yu, ACS Appl. Mater. Interfaces **4**, 1963 (2012).

35. F. Mokhtari, M. Latifi, M. Shamshirsaz, M. Khelghatdoost, and S. Rahmani, J. Text. Inst. **108**, 1917 (2017).

36. Z. Wei, H. Zhao, J. Zhang, L. Deng, S. Wu, J. He, and A. Dong, RSC Adv. **4**, 51381 (2014).

37. Y. J. Kim, H. I. Bae, O. K. Kwon, and M. S. Choi, Int. J. Biol. Macromol. **45**, 65 (2009).

38. A. I. Gopalan, K. P. Lee, K. M. Manesh, P. Santhosh, J.H. Kim, and J. S. Kang, Talanta **71**, 1774 (2007).

39. S. Raj and D. R. Shankaran, Sens. Actuators, B **226**, 318 (2016).

40. L. Buttafoco, N. G. Kolkman, B. P. Engbers, A. A. Poot, P. J. Dijkstra, I. Vermes, and J. Feijen, Biomaterials **27**, 724 (2006).

41. A. Baji, Y. W. Mai, Q. Li, and Y. Liu, Compos. Sci. Technol. **71**, 1435 (2011),

42. A. B. Hussain, Result. Phys. **4**, 69 (2014).

43. G. L. Haidar, I. A. Khalid, and H. A. Badran, Spectrochim. Acta, Part A **145**, 598 (2015).

44. A. B. Hussain, Am. J. Appl. Sci. **9**, 250 (2012).

45. B. Kadem, R. K. F. Alfahed, S. A. Ahmed, and A. B. Hussain, Optik **204**, 164153 (2020).

46. R. K. F. Alfahed, A. S. Al-Asadi, M. F. Al-Mudhaffer, and A. B. Hussain, Opt. Laser Technol., 106524 (2021).

47. R. K. F. Alfahed, A. B. Hussain, T. Y. A. Abu, and A. S. Noor, J. Phys. Conf. Ser. **1963**, 012136 (2021).

48. R. K. F. Alfahed, A. Dheyaa, Y. Zahraa, A. B. Hussain, and K. M. Kareem, Appl. Radiat. Isot. **196**, 110774 (2023).

49. A. B. Hussain, K. AL-Aladil, H. G. Lazim, and A. Y. Al-Ahmad, J. Mater. Sci.: Mater. Electron. **27**, 2212 (2016).

50. M. T. Obeed, R. C. H. AbuL-Hail, and H. A. Badran, J. Basrah Res. **46**, 49 (2020).

51. O. Muller, V. Pichot, L. Merlat, and D. Spitzer, Sci. Rep. **9**, 519 (2019).

52. R. K. F. Alfahed, I. Abdulameer, A. B. Hussain, and A. Abdalrahman, J. Mater. Sci.: Mater. Electron. **31**, 13862 (2020).

53. R. K. F. Alfahed, H. A. Badran, Y. A. Abu Talib, and A. S. Noor, J. Phys.: Conf. Ser. **1963**, 012136 (2021).

54. A. B. Hussain, A. Y. Al-Ahmad, M. F. Al-Mudhaffer, and A. E. Chassib, Opt. Quant. Electron. **47**, 1859 (2015).

55. H. A. Badran, A. A. F. Adil, R. K. F. Al-fahed, and S. A. Ahmed, J. Mater. Sci.: Mater. Electron. **28**, 17288 (2017).

56. F. A. Al-Saymari, A. B. Hussain, A. Y. Al-Ahmad, and A. E. Chassib, Indian J. Phys. **87**, 1153 (2013).

57. A. B. Hussain, C. H. A. Riyadh, and T. O. Mohammed, AIP Conf. Proc. **2290**, 050035 (2020).

58. A. B. Hussain, A. A. Hanan, R. K. F. Alfahed, and I. A. Khalid, J. Mater. Sci.: Mater. Electron. **32**, 14623 (2021).

59. A. Y. AL-Ahmad, M. F. AL-Mudhaffer, H. A. Badran, and C. A. Emshary, Opt. Laser Technol. **54**, 72 (2013).

60. A. B. Hussain, F. H. Hussain, and I. A. Khalid, Optik **127**, 5301 (2016).

61. H. A. Badran, Y. A. Abu Talib, and R. K. F. Al-Fahed, J. Phys.: Conf. Ser. **1963**, 012013 (2021).

62. A. Al-Salihi, R. D. Salim, R. K. F. Al-Fahed, and H. A. Badran, IOP Conf. Ser.: Mater. Sci. Eng. **928**, 072056 (2020).

63. K. F. A. Raed, A. Imran, M. S. Majeed, and A. B. Hussain, Phys. Scr. **95**, 075709 (2020).

64. H. A. Alhazam, R. K. F. Alfahed, A. Imran, H. A. Badran, S. S. Hussein, A. Alsalihi, and I. A. Khalid, J. Mater. Sci.: Mater. Electron. **30**, 10284 (2019).

65. A. B. Hussain, A. Y. Taha, A. F. Abdulkader, and C. A. Emshary, J. Ovonic Res. **8**, 161 (2012).

66. R. K. F. Alfahed, A. Imran, A. B. Hussain, and A. Al-Salihi, J. Mater. Sci.: Mater. Electron. **31**, 13862 (2020).

67. A. B. Hussain, A. Al-Maliki, R. K. F. Alfahed, B. A. Saeed, A. Y. Al-Ahmad, F. A. Al-Saymari, and R. S. Elias, J. Mater. Sci.: Mater. Electron. **29**, 10890 (2018).

68. R. Morvarid and D. Davoud, Rev. Adv. Mater. Sci. **40**, 110 (2015).

69. R. K. F. Alfahed, A. B. Hussain, Z. R. Fouad, and K. K. Mohammad, IOP Conf. Ser. Mater. Sci. Eng. **928**, 072071 (2020).

70. A. B. Hussain, I. A. Khalid, and H. G. Lazim, Mater. Res. Bull. **76**, 422 (2016).

71. A. T. Fadhil, T. O. Mohammed, A. J. Alyaa, A. B. Hussain, and T. A. Alaridhee, Result. Phys. **52**, 106858 (2023).

72. A. H. Abdullah, A. A. Musa, R. K. F. Alfahed, and A. B. Hussain, AIP Conf. Proc. **2290**, 050049 (2020).

73. R. K. F. Alfahed, S. A. Ahmed, A. B. Hussain, and I. A. Khalid, Appl. Phys. B **125**, 48 (2019).

74. H. A. Hasan, A. H. A. Nadia, A. B. Hussain, R. K. Alfahed, and I. A. Khalid, Opt. Quant. Electron. **55**, 555 (2023).

75. I. Litty, V. P. N. Nampoori, and P. Radhakrishnan, Sci. Adv. Mater. **2**, 578 (2010).

76. A. R. Azhr, H. A. Ali, A. M. Rajaa, and Z. A. Noor, IOP Conf. Ser. Mater. Sci. Eng. **928**, 072136 (2020).

77. U. Koji, M. Kohsuke, K. Erika, A. Norihisa, and S. Atsushi, ACS Appl. Mater. Interfaces **13**, 23049 (2021).

78. O. O. Marbello, S. D. Valbuena, and F. J. N. Racedo, J. Appl. Res. Technol. **18**, 333 (2020).

79. A. Mahsa, J. Babak, R. R. V. Mohammad, A. Wafaa, and S. V. Rajender, Pramana−J. Phys. **96**, 166 (2022).

80. A. H. A. Imad and A. A. Saif, Optik **126**, 4299 (2015).